Radiotherapy and Oncology xxx (2018) xxx–xxx

Contents lists available at ScienceDirect

Radiotherapy and Oncology

journal homepage: www.thegreenjournal.com

Original article

The EPTN consensus-based atlas for CT- and MR-based contouring in neuro-oncology

Daniëlle BP Eekers [a,b,*], Lieke in 't Ven [a], Erik Roelofs [a,c], Alida Postma [d], Claire Alapetite [e], Neil G. Burnet [f], Valentin Calugaru [g,h], Inge Compter [a], Ida E.M. Coremans [i,j], Morton Høyer [k], Maarten Lambrecht [l], Petra Witt Nyström [w,x], Alejandra Méndez Romero [j,m], Frank Paulsen [n], Ana Perpar [o], Dirk de Ruysscher [a,l], Laurette Renard [p], Beate Timmermann [y,z,aa], Pavel Vitek [q], Damien C. Weber [r], Hiske L. van der Weide [s], Gillian A. Whitfield [t,u], Ruud Wiggenraad [j,v], Esther G.C. Troost [ab,ac,ad,ae,af], on behalf of the taskforce "European Particle Therapy Network" of ESTRO

[a] *Department of Radiation Oncology (MAASTRO), GROW – School for Oncology and Developmental Biology, Maastricht University Medical Centre;* [b] *Proton Therapy Department South-East Netherlands (ZON-PTC), Maastricht;* [c] *The-D Lab: Decision Support for Precision Medicine, GROW – School for Oncology and Developmental Biology, Maastricht University Medical Centre+;* [d] *Department of Radiology and Nuclear Medicine MUMC+, Maastricht, The Netherlands;* [e] *Institut Curie, Radiation Oncology Department, Paris & Proton Center, Orsay, France;* [f] *University of Cambridge Department of Oncology, Addenbrooke's Hospital, United Kingdom;* [g] *Institute Curie, Paris;* [h] *Institute Curie, Centre de Protonthérapie d'Orsay, Orsay, France;* [i] *Leiden University Medical Centre, Department of Radiotherapy;* [j] *Holland Proton Therapy Centre, Delft, The Netherlands;* [k] *Danish Center for Particle Therapy, Aarhus, Denmark;* [l] *Department of Radiotherapy-Oncology, Leuven Kanker Instituut, UZ Gasthuisberg, Belgium;* [m] *Erasmus Medical Centre, Rotterdam, The Netherlands;* [n] *Department of Radiation Oncology, Eberhard-Carls-Universität Tübingen, Germany;* [o] *EBG MedAustron GmbH, Wiener Neustadt, Austria;* [p] *Service de Radiothérapie Oncologique Cliniques universitaires St Luc, Brussels, Belgium;* [q] *Proton Therapy Center Czech, Prague, Czech Republic;* [r] *Paul Scherrer Institut med. Center for Proton Therapy, Switzerland;* [s] *Department of Radiation Oncology, University Medical Center Groningen, University of Groningen, The Netherlands;* [t] *The University of Manchester, Manchester Academic Health Science Centre, The Christie NHS Foundation Trust;* [u] *The Children's Brain Tumour Research Network, University of Manchester, Royal Manchester Children's Hospital, United Kingdom;* [v] *Haaglanden Medisch Centrum, Department of Radiotherapy, Leidschendam, The Netherlands;* [w] *The Skandion Clinic, Uppsala;* [x] *Department of Immunology, Genetics and Pathology, Uppsala University, Sweden;* [y] *Clinic for Particle Therapy, University Hospital Essen, West German Cancer Center (WTZ);* [z] *West German Proton Therapy Center Essen (WPE);* [aa] *German Cancer Consortium (DKTK), partnersite Essen, Essen;* [ab] *Department of Radiation Oncology, Medical Faculty and University Hospital Carl Gustav Carus, Technische Universität Dresden;* [ac] *Institute of Radiooncology – OncoRay, Helmholtz-Zentrum Dresden - Rossendorf;* [ad] *OncoRay – National Center for Radiation Research in Oncology;* [ae] *German Cancer Consortium (DKTK), partnersite Dresden, Dresden, and German Cancer Research Center (DKFZ), Heidelberg; and* [af] *National Center for Tumor Diseases (NCT), partnersite Dresden, Dresden, Germany*

ARTICLE INFO

Article history:
Received 17 September 2017
Received in revised form 1 December 2017
Accepted 19 December 2017
Available online xxxx

Keywords:
Atlas for neuro-oncology
Organs at risk
Particle therapy
European Particle Therapy Network

ABSTRACT

Purpose: To create a digital, online atlas for organs at risk (OAR) delineation in neuro-oncology based on high-quality computed tomography (CT) and magnetic resonance (MR) imaging.
Methods: CT and 3 Tesla (3T) MR images (slice thickness 1 mm with intravenous contrast agent) were obtained from the same patient and subsequently fused. In addition, a 7T MR without intravenous contrast agent was obtained from a healthy volunteer. Based on discussion between experienced radiation oncologists, the clinically relevant organs at risk (OARs) to be included in the atlas for neuro-oncology were determined, excluding typical head and neck OARs previously published. The draft atlas was delineated by a senior radiation oncologist, 2 residents in radiation oncology, and a senior neuro-radiologist incorporating relevant available literature. The proposed atlas was then critically reviewed and discussed by European radiation oncologists until consensus was reached.
Results: The online atlas includes one CT-scan at two different window settings and one MR scan (3T) showing the OARs in axial, coronal and sagittal view. This manuscript presents the three-dimensional descriptions of the fifteen consensus OARs for neuro-oncology. Among these is a new OAR relevant for neuro-cognition, the posterior cerebellum (illustrated on 7T MR images).
Conclusion: In order to decrease inter- and intra-observer variability in delineating OARs relevant for neuro-oncology and thus derive consistent dosimetric data, we propose this atlas to be used in photon and particle therapy. The atlas is available online at www.cancerdata.org and will be updated whenever required.

* Corresponding author at: MAASTRO Clinic, Doctor Tanslaan 12, 6229 ET Maastricht, The Netherlands.
E-mail address: danielle.eekers@maastro.nl (D.BP Eeker.

https://doi.org/10.1016/j.radonc.2017.12.013
0167-8140/

In order to evaluate the added value of new radiotherapy (RT) modalities and techniques, such as particle therapy and adaptive highly conformal photon RT, it is essential to be able to accurately predict the individual patient's benefit in term of radiation-induced side effects [1–3]. The maturation and validation of normal tissue complication probability (NTCP) models are strongly dependent on uniform delineation of the relevant organs at risk (OARs), and reducing the inter- and intra-observer and trial protocol variability between clinicians and radiotherapy departments is an important objective. In this context, Brouwer et al. [4] and Kong et al. [5] published atlases for OARs relevant for head and neck and lung tumors, respectively.

During the last decade, several papers have been published on the delineation of OARs relevant to neuro-oncology both for adults and children [4,6,7]. These atlases may differ in minor details, but also some major discrepancies might occur, for instance, variations in the upper limit of the brainstem. Discrepancies in a critical OAR may influence the dose distribution and thus compromise the coverage of the target volume [4,6].

Within the Dutch Platform for Neuro-Oncology and the ESTRO taskforce "European Particle Therapy Network (EPTN)" there was a need to generate an atlas, which identifies the relevant OARs for neuro-oncology and can be used both for daily practice as well as research purposes [8]. With the ever-growing insight into the influence of radiotherapy on neurological functions, it is essential that this atlas can be easily updated when indicated.

Selection of OARs

In order to avoid overlap with existing head and neck atlases, typical head and neck OARs, which were previously published, were excluded from this consensus atlas [4]. All OARs at present known to be relevant for radiation-induced toxicity in neuro-oncology were included, namely: brain, brainstem, cochlea, vestibulum & semicircular canals, cornea, lens, retina, lacrimal gland, optic nerve, chiasm, pituitary, hippocampus and skin. In case of paired organs, each organ separately (left and right), and the unity of the two were contoured.

For future development of NTCP models, three distinct parts for the brainstem were defined, and regarding cognition, the posterior cerebellum, a new OAR possibly involved was included, as was the separation of the hippocampus into anterior and posterior parts. For research purposes also the hypothalamus was included. Of note, no validated dose–response curve relationships have thus far been published for these separate parts of the brainstem, hippocampus and cerebellum.

Uniform nomenclature

To facilitate future comparison of the structures, the proposed nomenclature is in accordance with work by Santanam et al. [9] on standardizing naming convention in radiation oncology, illustrated with quotes between brackets behind every structure name, for example: retina *("Retina_R", "Retina_L" and "Retinas").*

Delineation

The fifteen OARs introduced in several previous publications were delineated by the first author (DE) [4,6,7]. The anterior and posterior cerebellums were delineated by three authors (DE, LV, IC) using the high-resolution segment of the radiation treatment planning software (Eclipse™ v11.0 software, Varian, Palo Alto, CA). During a multi-disciplinary session, the senior radiation oncologist (DE), neuro-radiologist (AP), and two residents in radiation oncology (LV, IC) discussed the delineation of the OARs and came to consensus on a first draft atlas. This draft was then critically reviewed by Dutch and international experts in neuro-oncology and consensus on the final version of this atlas was reached.

Acquisition of CT and MR

CT images were acquired with intravenous contrast (Ultravist®, 150 ml of 300 mg Iodine per mL, 2 mL per sec, 5 min delay, slice thickness 1 mm, 50 cm field of view, 120 kV, 685 mAs) using window-width/window-level settings (WW/WL) of 120/40 and 120/1500 (SOMATOM Sensation 10, Siemens Healthcare, Erlangen, Germany) of the head of an adult male low grade glioma patient after first resection. Moreover, a three-dimensional spoiled gradient (3D-SPGR) axial 3T MR scan (1 mm slice thickness) of the same patient in standard axial, sagittal and coronal reconstruction, and an axial T2- and a gadolinium (Gadovist® 1.0 mmol/ml 0.1 mL/kg bodyweight) contrast-enhanced axial T1-weighted sequence were acquired, with sagittal and coronal reconstruction. Both CT and MR were obtained in the supine position with the head in a neutral position; immobilization devices routinely used in radiation therapy were used for CT acquisition. Rigid MR-CT co-registration and delineation were performed using the Eclipse™ treatment planning system with the high-resolution segment.

For illustration purposes, 7T MR images of a healthy volunteer were acquired (Siemens Magnetom 7T) with a slice thickness of 0.7 mm using a 32-channel head coil (Nova Medical Inc., Wilmington, CA; Fig. 1). The magnetization-prepared rapid gradient-echo (MP2RAGE) was selected for OAR delineation due to its superior soft tissue contrast (Fig. 2). Scan parameters have previously been published by Compter et al. [10]. Vendor-based 3D distortion correction methods were applied.

Three-dimensional description of the OARs

Cornea ("Cornea_R", "Cornea_L" and "Corneas")

The cornea is located at the anterior segment of the eyeball consisting of the structures ventral to the vitreous humor, the iris, ciliary body, and lens [6]. Using a brush of 2–3 mm the cornea can easily be delineated on MR as well as CT.

Retina ("Retina_R", "Retina_L" and "Retinas")

The retina is a neurosensorial membrane of 2–3 mm thickness, located at the posterior part of the eyeball, posterior to the cornea and lens, and is the innermost of the three layers that form the wall of the eyeball (sclera, uvea/choroid and retina). Using a 3 mm brush, it can be delineated on MR as well as CT as a membrane covering the posterior 5/6 of the globe, extending nearly as far as the ciliary body. The anterior border of the retina is between the insertion of the medial rectus muscle and the lateral rectus muscle, posterior to the ciliary body. The optic nerve is excluded from this contour [4,6].

Lacrimal gland ("LacrimalGland L", "LacrimalGland_R" and "LacrimalGlands")

The lacrimal gland is an almond shaped gland (18 mm craniocaudally, 15 mm axial length and 5 mm axial width) located in the orbit superior-lateral to the eye, superior to the lateral rectus muscle and lateral to the superior rectus muscle. It can be delineated on CT using soft brain 120/40 or soft tissue 350/50 WW/WL settings [4,6,11].

Please cite this article in press as: Eekers DB et al. The EPTN consensus-based atlas for CT- and MR-based contouring in neuro-oncology. Radiother Oncol (2018), https://doi.org/10.1016/j.radonc.2017.12.013

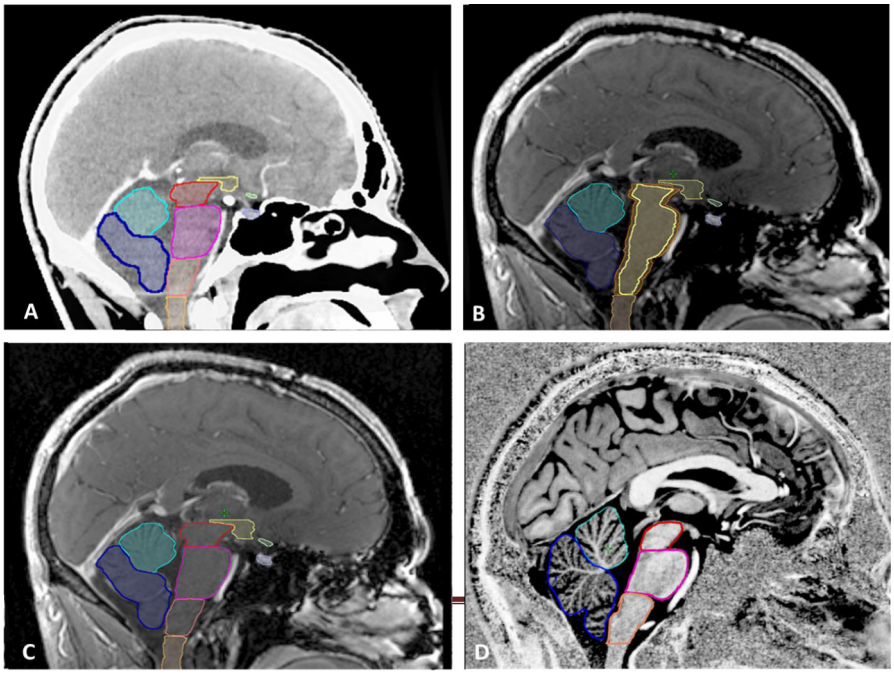

Fig. 1. Sagittal (midline) view of the delineation. (A) Sagittal CT image (WL 140/40), (B + C) sagittal 3 Tesla MRI (T1 with gadolinium), (D) sagittal 7 Tesla MRI. Light blue = cerebellum anterior, dark blue = cerebellum posterior, red = midbrain, magenta = pons, pink = medulla oblongata, orange = spinal cord, light yellow = hypothalamus, green = chiasm, purple = pituitary, orange = brainstem surface, yellow = brainstem interior. (For interpretation of the references to color in this figure legend, the reader is referred to the web version of this article.)

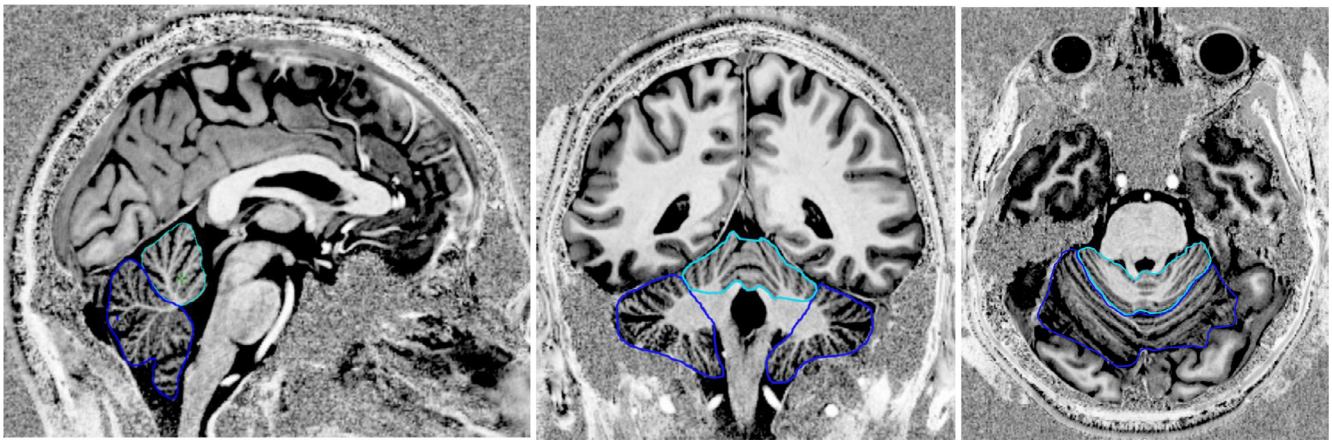

Fig. 2. Sagittal (midline) view of cerebellum delineation on 7 Tesla MRI. From left to right: 7 Tesla MRI, sagittal, coronal and transversal. Light blue = cerebellum anterior, dark blue = cerebellum posterior.

Lens of the Eye ("Lens_R", "Lens_L" and "Lenses")

The lens (diameter up to 10 mm) is a clearly visible biconvex avascular structure, located between the vitreous humor and the iris and can easily be delineated on CT [6]. It should be taken into account that without instructing the patient, the position of the lens is not fixed and can vary during treatment.

Optic nerve ("OpticNerve_R", "OpticNerve_L" and "OpticNerves")

The optic nerve (2–5 mm thick) is delineated from the posterior edge of the eyeball, through the bony optic canal, where it narrows slightly, to the optic chiasm. Close to the optic chiasm, an MR scan (T1 weighted) is recommended for better delineation of the optic nerve. Contouring the optic nerve in continuity with the chiasm is crucial for dose reporting purposes, as dose gradients can be very steep with modern photon and proton techniques [4,12].

Optic chiasm ("Chiasm")

The optic chiasm (14 mm transverse, 8 mm antero-posterior and 2–5 mm thick) is located 1 cm superior to the pituitary gland, which has high signal on T1 MRI, and just anterior to the pituitary stalk (located above the sella turcica). The lateral border is the internal carotid artery. The chiasm is superiorly located in the antero-inferior part of the third ventricle, below the supra-optic recess and above the infundibular recess of the third ventricle, with the optic nerves in front and the divergence of the optic tracts behind. The anterior cerebral arteries and the anterior communicating artery are located ventral to the chiasm. A T1 weighted

Please cite this article in press as: Eekers DB et al. The EPTN consensus-based atlas for CT- and MR-based contouring in neuro-oncology. Radiother Oncol (2018), https://doi.org/10.1016/j.radonc.2017.12.013

MR (axial, sagittal and coronal) is recommended for delineation of the optic chiasm [4,6].

Pituitary gland ("Pituitary")

The pituitary gland cannot be easily identified on axial CT, although the bony margins of the fossa are well shown. It is oval-shaped (craniocaudally up to 12 mm) and lies in the sella turcica. Laterally, the pituitary gland is bordered by the cavernous sinuses, which are well visible with intravenous contrast agent, it is just inferior to the brain, and is connected to the hypothalamus by its pituitary stalk. The borders of the pituitary gland can be defined best in the sagittal view [4,5]. Alternatively, the inner part of the sella turcica can be used as a surrogate anatomical bony structure best identified using bone 1500/950 or soft tissue 350/50 WL/WW on CT.

Hypothalamus ("Hypothalamus_R, "Hypothalamus_L" and "Hypothalami")

The hypothalamus (2–4 cm^3) is a polygonal structure consisting of two separate volumes on each side of the third ventricle, delineated using MR-based anatomic landmarks representing surrogate boundaries for the hypothalamus itself. The superior boundaries are the axial slices containing the anterior and the posterior commissure. Inferiorly, the boundary consists of the base of the third ventricle or the visible edge of the cerebrospinal fluid (CSF) space within the suprasellar cistern, while posteriorly the contour reaches to the level of the interpeduncular fossa. The mammillary bodies should be included in the contour. The medial border consists of the third ventricle or the visible CSF space. Since the lateral border is not clearly visible, the contour was bounded laterally 3 mm from the third ventricle. Delineation on a T1 weighted MR is strongly recommended [13–16].

Hippocampus ("Hippocampus_P_R", "Hippocampus_P_L", "Hippocampus_A_R", "Hippocampus_A_L", and "Hippocampi")

The literature describes considerable age- and disease-specific variability in hippocampal size (range 2.8–4.0 cm^3) and location [7,17–19]. The hippocampus (HC) is delineated as the gray matter medial to the medial boundary of the temporal horn of the lateral ventricle, bordered medially by the quadrigeminal cistern as described by Gondi et al. [7]. Blum et al. [20] suggest a separation of the HC into a posterior (corpus) and anterior (head) part using the lateral ventricle as dorsal border for the anterior hippocampus. In sagittal view, the head of the HC is separated from the body at the narrowing of the HC, with the uncus located dorsally [20,21]. Delineation on MR (T1 weighted) is essential.

Cochlea ("Cochlea_R", "Cochlea_L" and "Cochleas")

The cochlea is a spiral structure (up to 0.6 cm^3) located in a bony cavity in the petrous portion of the temporal bone, caudal to the semicircular canals, lateral to the internal auditory canal. Using a WW/WL setting of 120/1500 on CT images, its volume can be defined as a small cavity. The structures of the inner ear are well visible on MR (T2 weighted) images [4,6]. The semicircular canals should not be included.

Vestibular and semicircular canal ("VSCC_R", "VSCC_L", "VSCCs")

As the semicircular canals are a part of the bony labyrinth with the superior, posterior and lateral canals aligned in three planes, delineation is advised using the bone setting on CT images (WW/WL 120/1500). The semicircular canal is located laterally and cranially of the cochlea. The canals are also visible as small cavities on MR (T2 weighted) [6].

Brain Stem ("BrainStem", "Brainstem_surface", "Brainstem_interior" or "Midbrain", "Pons" and "Medulla Oblongata")

The brainstem is to be contoured on MR images and can be divided into three parts, from cranial to caudal, the midbrain, pons and medulla oblongata. The midbrain is defined from the nigral substance at the cerebral peduncle to the upper border of the pons. The pons is an oval shaped structure on sagittal views, which is easy to discriminate (see Fig. 1C). The caudal limit of the medulla oblongata is the tip of the dens of C2 (*i.e.*, the odontoid peg), which is also the cranial border of the spinal cord; the cranial limit is the ponto-medullary junction [4,6,22]. For practical reason the cerebral aqueduct is included until it becomes the 4th ventricle. The brainstem interior is the brainstem surface contour cropped by 2 mm (inner border). The brainstem surface is the brainstem excluding the brainstem interior [23,24]. These structures are contoured automatically (and checked thereafter) using a built-in delineation tool commonly found in treatment planning systems.

Brain ("Brain" and "Brain_Supratentorial")

The delineation of the brain includes the cerebellum, CSF and small brain vessels, and excludes the brainstem and large cerebellar vessels, such as the sigmoid sinus, transverse sinus and superior sagittal sinus (Fig. 3C). For delineation purposes, CT in brain soft tissue 350/40 WW/WL-settings is recommended. Alternatively, the brain can be contoured automatically (and checked thereafter) using a built-in delineation tool commonly found in the majority of treatment planning systems [4,6,25]. In the middle cranial fossa the carotid canal and cavernous sinuses, most easily seen on contrast-enhanced T1 MRI, should not be included. The supratentorial brain equals the "Brain" excluding the cerebellum (see Section "Cerebellum ("Cerebellum_P", "Cerebellum_A' and "Cerebellum")").

Cerebellum ("Cerebellum_P", "Cerebellum_A' and "Cerebellum")

The separation of the cerebellum into an anterior and posterior part is best seen on the sagittal T1 weighted MR (see Fig. 1). The anterior cerebellum consists of the cranial part of the cerebellum including half of the medullary corpus. The posterior cerebellum consists of the caudal and posterior part of the cerebellum with a cranial border including the lower half of the medullary corpus. This part includes the flocculonodular lobe. The primary fissure, which is best seen on 7-Tesla MR (see Fig. 2), divides the anterior part from the posterior part of the cerebellum [26]. The lateral borders for both parts are the large vessels (the sigmoid sinus, transverse sinus and superior sagittal sinus) and CSF, which are both excluded.

Skin ("Skin")

The skin is the volume defined by the body contour (outer border) and the body contour cropped by 5 mm (inner border), both created on the CT. This structure is contoured automatically (and checked thereafter) using a built-in delineation tool commonly found in treatment planning systems [4,6,25].

All mentioned OARs are delineated on CT and MR (see Fig. 3) in an easily accessible delineation atlas at www.cancerdata.org [27].

Please cite this article in press as: Eekers DB et al. The EPTN consensus-based atlas for CT- and MR-based contouring in neuro-oncology. Radiother Oncol (2018), https://doi.org/10.1016/j.radonc.2017.12.013

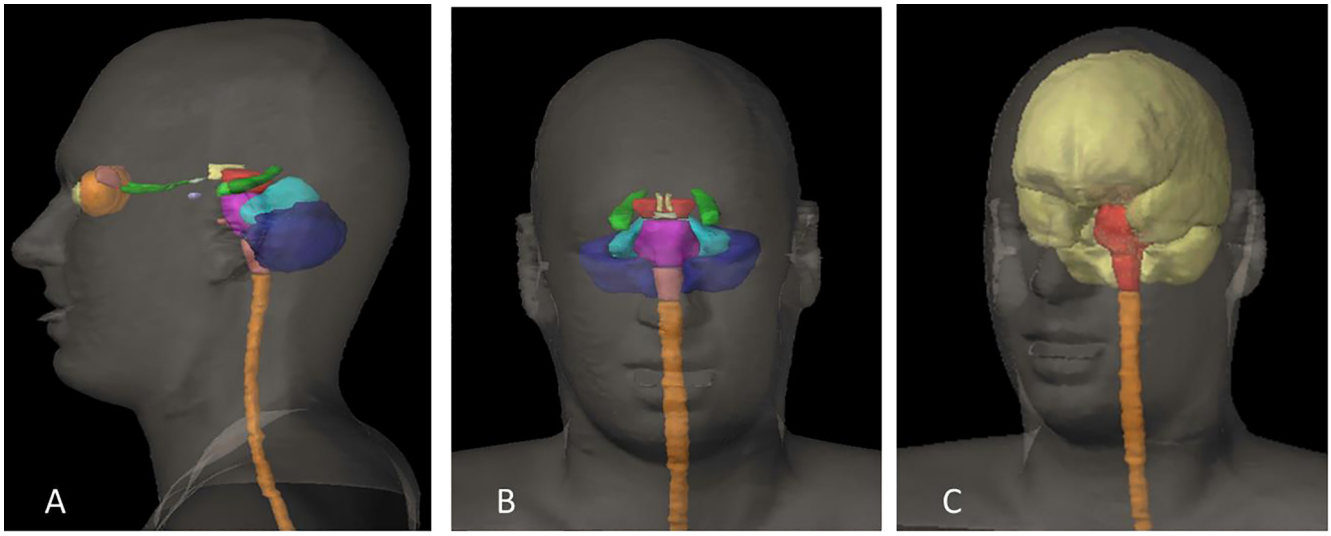

Fig. 3. 3D view of the OARs delineation on CT. (A) From ventral to dorsal: yellow = cornea, orange = retina, brown = lacrimal gland, green = optic nerve, light green = chiasm, purple = pituitary, yellow (central) = hypothalamus, red = midbrain, green (central) = hippocampus anterior, dark green = hippocampus posterior, pink = cochlea, magenta = pons, pink = medulla oblongata, orange = spinal cord, light blue = cerebellum anterior, dark blue = cerebellum posterior. (B) From cranial to caudal: yellow = hypothalamus, red = midbrain, light green = chiasm, green = hippocampus anterior, dark green = hippocampus posterior, magenta = pons, pink = medulla oblongata, Light blue = anterior cerebellum, dark blue = posterior cerebellum, orange = spinal cord. (C) Yellow = brain, red = brainstem, orange = spinal cord. (For interpretation of the references to color in this figure legend, the reader is referred to the web version of this article.)

Discussion

The presented atlas for contouring OARs involved in neuro-oncology aims at reducing the inter- and intra-observer delineation variability and thus enabling more consistent plan comparison. This is especially relevant when comparing different radiation treatment techniques and modalities, and for establishing detailed dose–response relationships and NTCP models for different OARs.

Toxicity to the optical system is a feared complication especially when it results in partial or total loss of vision or pain to the eye. Despite their small volume, a separate delineation of the different optical structures is crucial in order to derive dose–volume histograms and predict post-radiation toxicity. The optic chiasm is an anatomically cross-shaped structure, as is depicted by Scoccianti et al. [6] and not round as presented in the atlas by Brouwer et al. [4]. Moreover, the chiasm should be contoured in continuity with both optic nerves in order to prevent high-dose deposits in un-delineated voxels. The retina is to be delineated separately from the vitreous body, since radiation induced retinopathy can be treated if observed in an early state. Consequently, correct dose calculation is of utmost relevance in order to refer a patient suffering from this radiation induced side-effect [28]. Separate delineation of the cornea is proposed since toxicity and tolerance dose differ from that of the retina [4,28,29]. Damage to the cornea, radiation keratitis, is painful and deteriorates sight. The mean radiation dose to the lacrimal gland is related to the development of a dry eye, which can be painful and render the eye susceptible to infections [28]. A cataract can develop at a rather low dose to the lens. This side-effect can be alleviated by surgical implantation of an artificial lens [28]. A normal lens is well seen because of its high protein content, whereas an artificial lens is difficult to see on CT or MR, but since it tolerates radiation dose, delineation is not required.

Hypo-pituitarism may take a long time to be diagnosed since its symptoms can be vague. Depending on the mean dose to the pituitary gland, an early referral to an endocrinologist can facilitate early initiation of treatment and thus prevent impaired quality of life [30,31]. In general, it is advised to delineate the entire sella content to be sure the whole pituitary is included rather than the central part only, excluding the suprasellar part of the infundibulum [4,6]. Even though there are no established dose constraints for the hypothalamus available yet, we believe that these data need to be collected in a prospective manner, in order to correlate levels of hormone production and regulation of metabolic processes with delivered radiation dose.

Hearing preservation after radiotherapy is known to be related to dose to the cochlea [32–34]. There is agreement in the literature on its delineation, most optimally done on a CT scan with thin slices using a bone WW/WL-setting considering its location in the mastoid bone [4,6]. Since dizziness is a side-effect occasionally reported after radiotherapy it was decided to delineate the semicircular canals as well, using the same WW/WL-settings as for the cochlea, although future data are needed to establish a validated dose constraint.

Recent literature has shown some dose–response relationship between the hippocampus and cognition as described by Gondi et al. [34] using the absolute radiation dose to 40% of both hippocampi (D40%). We firmly encourage delineating the hippocampi separately and into anterior and posterior parts, since the left hippocampus is known to be dominant in most patients (including left-handed patients) for verbal memory, and the right hippocampus for non-verbal memory also known as visual memory. Moreover, the posterior parts of the hippocampi are more related to memory than the anterior parts [35–39].

The brain is often automatically delineated and for practical reasons the included small vessels are left in the contour since editing the contour would be too time consuming. There are dose constraints for brain tissue, especially on high doses related to temporal lobe radionecrosis in head and neck cancer patients [40–45]. Regarding neuro-cognition, some publications on pediatric patients have shown a correlation between low dose radiation to the supra-tentorial brain and cognitive decline [40,46]. Further data are needed to transfer this knowledge to adult patients. Data on whole brain radiotherapy and prophylactic cranial irradiation have hinted at the negative effect of low dose on cognition [47–54]. However, there still is a strong need for an adult NTCP model on brain tissue and cognition.

Symptomatic brainstem necrosis is a feared, but rare complication following radiotherapy to the brain [55,56]. It was decided to contour the brainstem in three anatomically distinct parts, because some hypothesize that specific volumes within the brainstem are

Please cite this article in press as: Eekers DB et al. The EPTN consensus-based atlas for CT- and MR-based contouring in neuro-oncology. Radiother Oncol (2018), https://doi.org/10.1016/j.radonc.2017.12.013

more sensitive to radiation than others. In particle beam therapy, the anterior surface and center of the brainstem are delineated separately since a higher tolerance at the surface of the brainstem has been observed [23,24]. This should be subject to further research for both photon and particle radiotherapy.

The delineation of the cerebellum is also added as a possible new OAR for research purposes, since there are data suggesting a relationship between the posterior cerebellum and cognition [57]. Cantelmi et al. [58] state that recognition of the important cognitive contributions of the cerebellum might lead to improved cognitive outcome and quality of life. This definitely needs further research into a possible dose–response relationship and tolerance dose, which is only possible when agreement is reached in the delineation, as proposed based on Schmahmann et al. [26,55,58].

For radiation treatment planning purposes, the skin is added as an OAR since alopecia and erythema are disturbing side-effects. Using the skin structure enables lowering the dose during treatment planning, which is of particular importance in proton therapy with its relatively high entry dose [59].

A limitation of the atlas is the fact that the three dimensional angulation possibilities in a radiation treatment planning systems are often limited and patients are mostly not aligned perfectly in the midline. This is why the atlas was based on a random CT/MR-dataset of an imperfectly aligned patient, resembling routine clinical practice. The atlas includes transversal, coronal and sagittal views to assist the delineation process. A second potential limitation of this atlas is that we had to limit the number of OARs proposed for otherwise the atlas would have been impracticable and thus not used in routine clinical practice. Future research should unravel the role of additional OARs and the NTCP value for: Eustachian tube, circle of Willis, optic tract, frontal & temporal lobe, anterior eye chambers, macula, mammillary bodies, spinal canal and cerebrospinal space. Thirdly, this atlas does not summarize the available literature on dose constraints for the contoured organs at risk; this enormous effort will be a separate project of the EPTN. Finally, even though this atlas was contoured on a 3T MR scan, it can be easily transferred to 1.5T MR images.

Uniform contouring of structures in the central nervous system, both in photon and particle therapy, is considered important for: (1) the generalization of normal tissue dose constraints, (2) establishment or update of NTCP models taking into account new radiation treatment techniques, and (3) for comparative multicenter clinical studies on radiotherapy in patients with primary brain tumors. Besides uniform contouring, consensus on OAR dose constraints is also required for implementing and improving NTCP models. A separate article on dose constraints for the given OARs, again consented by the EPTN, is currently being prepared.

Conclusion

In order to decrease variability in delineating OARs involved in neuro-oncology and to allow the generation of consistent dosimetric data, we propose an atlas for neuro-oncology including some new OARs in order to give an anatomical basis for the development of international acknowledged constraints and volumes. This will enable the community to amplify existing and new NTCP models such that more accurate prediction, and possibly prevention, of long-term radiation toxicity comes within reach. The atlas is available online on www.cancerdata.org and will be updated whenever required.

Acknowledgement

The authors sincerely thank all the members of the Dutch Platform for Radiation in Neuro-Oncology for their input and consensus, and they thank Marlies Granzier, radiation technologist at MAASTRO clinic for her expertise and support with data transfer and image fusion. NGB is supported by the National Institute for Health Research Cambridge Biomedical Research Centre.

Disclosure of conflicts of interest

This research was partially supported by the Brains Unlimited Pioneer Fund of the Limburg University Fund/SWOL (S.2013.1.011).

Ethical publication statement

We confirm that we have read the Journal's position on issues involved in ethical publication and affirm that this report is consistent with those guidelines.

References

[1] Eekers DB, Roelofs E, Jelen U, Kirk M, Granzier M, Ammazzalorso F, et al. Benefit of particle therapy in re-irradiation of head and neck patients. Results of a multicentric in silico ROCOCO trial. Radiother Oncol 2016;121:387–94.
[2] Roelofs E, Engelsman M, Rasch C, Persoon L, Qamhiyeh S, de Ruysscher D, Verhaegen F, Pijls-Johannesma M, Lambin P. ROCOCO Consortium. Results of a multicentric in silico clinical trial (ROCOCO): comparing radiotherapy with photons and protons for non-small cell lung cancer. J Thorac Oncol 2012;7:165–76.
[3] van der Laan HP, van de Water TA, van Herpt HE, Christianen ME, Bijl HP, Korevaar EW, Rasch CR, van 't Veld AA, van der Schaaf A, Schilstra C, Langendijk JA, Rococo cooperative group. The potential of intensity-modulated proton radiotherapy to reduce swallowing dysfunction in the treatment of head and neck cancer: A planning comparative study. Acta Oncol 2013;52:561–9.
[4] Brouwer CL, Steenbakkers RJ, Bourhis J, Budach W, Grau C, Grégoire V, et al. CT-based delineation of organs at risk in the head and neck region: DAHANCA, EORTC, GORTEC, HKNPCSG, NCIC CTG, NCRI, NRG Oncology and TROG consensus guidelines. Radiother Oncol 2015;117:83–90.
[5] Kong FM, Ritter T, Quint DJ, Senan S, Gaspar LE, Komaki RU, et al. Consideration of dose limits for organs at risk of thoracic radiotherapy: atlas for lung, proximal bronchial tree, esophagus, spinal cord, ribs, and brachial plexus. Int J Radiat Oncol Biol Phys 2011;81:1442–57.
[6] Scoccianti S, Detti B, Gadda D, Greto D, Furfaro I, Meacci F, et al. Organs at risk in the brain and their dose-constraints in adults and in children: a radiation oncologist's guide for delineation in everyday practice. Radiother Oncol 2015;114:230–8.
[7] Gondi V, Tolakanahalli R, Mehta MP, Tewatia D, Rowley H, Kuo JS, et al. Hippocampal-sparing whole-brain radiotherapy: A "howto" technique, utilizing helical tomotherapy and LINAC-based intensity modulated radiotherapy. Int J Radiat Oncol Biol Phys 2010;78:1244–52.
[8] Weber DC, Abrunhosa-Branquinho A, Bolsi A, Kacperek A, Dendale R, Geismar D, et al. Profile of European proton and carbon ion therapy centers assessed by the EORTC facility questionnaire. Radiother Oncol 2017;124:185–9.
[9] Santanam L, Hurkmans C, Mutic S, van Vliet-Vroegindeweij C, Brame S, Straube W, et al. Standardizing naming conventions in radiation oncology. Int J Radiat Oncol Biol Phys 2012;83:1344–9.
[10] Compter I, Peerlings J, Eekers DB, Postma AA, Ivanov D, Wiggins CJ, et al. Technical feasibility of integrating 7 T anatomical MRI in image-guided radiotherapy of glioblastoma: a preparatory study. MAGMA 2016;29:591–603.
[11] Bulbul E, Yazici A, Yanik B, Yazici H, Demirpolat G. Evaluation of lacrimal gland dimensions and volume in turkish population with computed tomography. J Clin Diagn Res 2016;10:TC06-8.
[12] Celesia GG, DeMarco Jr PJ. Anatomy and physiology of the visual system. J Clin Neurophysiol 1994;11:482–92 [Review].
[13] Merchant TE, Goloubeva O, Pritchard DL, Gaber MW, Xiong X, Danish RK, et al. Radiation dose-volume effects on growth hormone secretion. Int J Radiat Oncol Biol Phys 2002;52:1264–70.
[14] Elson A, Bovi J, Kaur K, Maas D, Sinson G, Schultz C. Effect of treatment modality on the hypothalamic-pituitary function of patients treated with radiation therapy for pituitary adenomas: hypothalamic dose and endocrine outcomes. Front Oncol 2014;9:73.
[15] Rappaport R, Brauner R. Growth and endocrine disorders secondary to cranial irradiation. Pediatr Res 1989;25:561–7 [Review].
[16] Baroncini M, Jissendi P, Balland E, Besson P, Pruvo JP, Francke JP, et al. MRI atlas of the human hypothalamus. Neuroimage 2012;59:168–80.
[17] Chera BS, Amdur RJ, Patel P, Mendenhall WM. A radiation oncologist's guide to contouring the hippocampus. Am J Clin Oncol 2009;32:20–2.
[18] Konrad C, Ukas T, Nebel C, Arolt V, Toga AW, Narr KL. Defining the human hippocampus in cerebral magnetic resonance images. An overview of current segmentation protocols. Neuroimage 2009;47:1185–95.
[19] Bender ET, Mehta MP, Tomé WA. On the estimation of the location of the hippocampus in the context of hippocampal avoidance whole brain radiotherapy treatment planning. Technol Cancer Res Treat 2009;8:425–32.

Please cite this article in press as: Eekers DB et al. The EPTN consensus-based atlas for CT- and MR-based contouring in neuro-oncology. Radiother Oncol (2018), https://doi.org/10.1016/j.radonc.2017.12.013

[20] Blum S, Habeck C, Steffener J, Razlighi Q, Stern Y. Functional connectivity of the posterior hippocampus is more dominant as we age. Cogn Neurosci 2014;5:150–9.
[21] Sivakumar PT, Kalmady SV, Venkatasubramanian G, Bharath S, Reddy NN, Rao NP, et al. Volumetric analysis of hippocampal sub-regions in late onset depression: a 3 tesla magnetic resonance imaging study. Asian J Psychiatr 2015;13:38–43.
[22] Kocak-Uzel E, Gunn GB, Colen RR, et al. Beam path toxicity in candidate organs-at-risk: Assessment of radiation emetogenesis for patients receiving head and neck intensity modulated radiotherapy. Radiother Oncol 2014;111:281–8.
[23] Noël G, Habrand JL, Mammar H, Haie-Meder C, Pontvert D, Dederke S, et al. Highly conformal therapy using proton component in the management of meningiomas. Preliminary experience of the Centre de Protonthérapie d'Orsay. Strahlenther Onkol 2002;178(9):480–5.
[24] Feuvret L, Bracci S, Calugaru V, Bolle S, Mammar H, De Marzi L, et al. Efficacy and safety of adjuvant proton therapy combined with surgery for chondrosarcoma of the skull base: a retrospective, population-based study. Int J Radiat Oncol Biol Phys 2016;95:312–21.
[25] Sun Y, Yu X-L, Luo W, et al. Recommendation for a contouring method and atlas of organs at risk in nasopharyngeal carcinoma patients receiving intensity-modulated radiotherapy. Radiother Oncol 2014;110:390–7.
[26] Schmahmann JD, Doyon J, McDonald D, Holmes C, Lavoie K, Hurwitz AS, et al. Three-dimensional MRI atlas of the human cerebellum in proportional stereotaxic space. Neuroimage 1999;10:233–60.
[27] Eekers DBP, in 't Ven L, Roelofs E, Postma A, Troost EGC. EPTN International Neurological Contouring Atlas. CancerData 2017. https://doi.org/10.17195/candat.2017.08.1.
[28] Jeganathan VS, Wirth A, MacManus MP. Ocular risks from orbital and periorbital radiation therapy: a critical review. Int J Radiat Oncol Biol Phys 2011;79:650–9.
[29] Barabino S, Raghavan A, Loeffler J, Dana R. Radiotherapy-induced ocular surface disease. Cornea 2005;24:909–14 [Review].
[30] De Marzi L, Feuvret L, Boulé T, Habrand JL, Martin F, Calugaru V, et al. Use of gEUD for predicting ear and pituitary gland damage following proton and photon radiation therapy. Br J Radiol 2015;88:20140413.
[31] Darzy KH, Shalet SM. Hypopituitarism following Radiotherapy Revisited. Endocr Dev 2009;15:1–24.
[32] Bhandare N, Jackson A, Eisbruch A, Pan CC, Flickinger JC, Antonelli P, et al. Radiation therapy and hearing loss. Int J Radiat Oncol Biol Phys 2010;76: S50–7.
[33] Mujica-Mota M, Waissbluth S, Daniel SJ. Characteristics of radiation-induced sensorineural hearing loss in head and neck cancer: a systematic review. Head Neck 2013;35:1662–8.
[34] Gondi V, Hermann BP, Mehta MP, Tomé WA. Hippocampal dosimetry predicts neurocognitive function impairment after fractionated stereotactic radiotherapy for benign or low-grade adult brain tumors. Int J Radiat Oncol Biol Phys 2012;83:e487–93.
[35] Greene-Schloesser D, Moore E, Robbins ME. Molecular pathways: radiation-induced cognitive impairment. Clin Cancer Res 2013;19:2294–300.
[36] Tsai PF, Yang CC, Chuang CC, Huang TY, Wu YM, Pai PC, et al. Hippocampal dosimetry correlates with the change in neurocognitive function after hippocampal sparing during whole brain radiotherapy: a prospective study. Radiat Oncol 2015;10:253.
[37] Blum S, Habeck C, Steffener J, Razlighi Q, Stern Y. Functional connectivity of the posterior hippocampus is more dominant as we age. Cogn Neurosci 2014;5:150–9.
[38] Poppenk J, Moscovitch M. A hippocampal marker of recollection memory ability among healthy young adults: contributions of posterior and anterior segments. Neuron 2011;72:931–7.
[39] Lee AW, Foo W, Chappell R, Fowler JF, Sze WM, Poon YF, et al. Effect of time, dose, and fractionation on temporal lobe necrosis following radiotherapy for nasopharyngeal carcinoma. Int J Radiat Oncol Biol Phys 1998;40:35–42.
[40] Armstrong GT, Jain N, Liu W, Merchant TE, Stovall M, Srivastava DK, et al. Region-specific radiotherapy and neuropsychological outcomes in adult survivors of childhood CNS malignancies. Neuro Oncol 2010;12:1173–86.
[41] Marks LB, Yorke ED, Jackson A, Ten Haken RK, Constine LS, Eisbruch A, et al. Use of normal tissue complication probability models in the clinic. Int J Radiat Oncol Biol Phys 2010;76:S10–9.
[42] Su SF, Huang SM, Han F, Huang Y, Chen CY, Xiao WW, et al. Analysis of dosimetric factors associated with temporal lobe necrosis (TLN) in patients with nasopharyngeal carcinoma (NPC) after intensity modulated radiotherapy. Radiat Oncol 2013;22:17.
[43] Hsu YC, Wang LF, Lee KW, Ho KY, Huang CJ, Kuo WR. Cerebral radionecrosis in patients with nasopharyngeal carcinoma. Kaohsiung J Med Sci 2005;21:452–9.
[44] Zeng L, Huang SM, Tian YM, Sun XM, Han F, Lu TX, et al. Normal tissue complication probability model for radiation-induced temporal lobe injury after intensity-modulated radiation therapy for nasopharyngeal carcinoma. Radiology 2015;276:243–9.
[45] Mulhern RK, Fairclough D, Ochs J. A prospective comparison of neuropsychologic performance of children surviving leukemia who received 18-Gy, 24-Gy, or no cranial irradiation. J Clin Oncol 1991;9:1348–56 [Erratum in: J Clin Oncol 1991 Oct;9(10):1922].
[46] Mulhern RK, Kepner JL, Thomas PR, Armstrong FD, Friedman HS, Kun LE. Neuropsychologic functioning of survivors of childhood medulloblastoma randomized to receive conventional or reduced-dose craniospinal irradiation: a Pediatric Oncology Group study. J Clin Oncol 1998;16:1723–8.
[47] Peiffer AM, Leyrer CM, Greene-Schloesser DM, Shing E, Kearns WT, Hinson WH, et al. Neuroanatomical target theory as a predictive model for radiation-induced cognitive decline. Neurology 2013;80:747–53.
[48] Ravn S, Holmberg M, Sørensen P, Frøkjær JB, Carl J. Differences in supratentorial white matter diffusion after radiotherapy–new biomarker of normal brain tissue damage? Acta Oncol 2013;52:1314–9.
[49] Gregor A, Cull A, Traynor E, Stewart M, Lander F, Love S. Neuropsychometric evaluation of long-term survivors of adult brain tumours: relationship with tumour and treatment parameters. Radiother Oncol 1996;41:55–9.
[50] Tallet AV, Azria D, Barlesi F, Spano JP, Carpentier AF, Gonçalves A, et al. Neurocognitive function impairment after whole brain radiotherapy for brain metastases: actual assessment. Radiat Oncol 2012;28:77.
[51] Gan HK, Bernstein LJ, Brown J, Ringash J, Vakilha M, Wang L, et al. Cognitive functioning after radiotherapy or chemoradiotherapy for head-and-neck cancer. Int J Radiat Oncol Biol Phys 2011;81:126–34.
[52] Makale MT, McDonald CR, Hattangadi-Gluth JA, Kesari S. Mechanisms of radiotherapy-associated cognitive disability in patients with brain tumours. Nat Rev Neurol 2017;13:52–64.
[53] Edelstein K, Richard NM, Bernstein LJ. Neurocognitive impact of cranial radiation in adults with cancer: an update of recent findings. Curr Opin Support Palliat Care 2017;11:32–7.
[54] Shih HA, Sherman JC, Nachtigall LB, Colvin MK, Fullerton BC, Daartz J, et al. Proton therapy for low-grade gliomas: Results from a prospective trial. Cancer. 2015;121:1712–9.
[55] Mayo C, Yorke E, Merchant TE. Radiation associated brainstem injury. Int J Radiat Oncol Biol Phys 2010;76:S36–41.
[56] DeSalvo MN. Radiation necrosis of the pons after radiotherapy for nasopharyngeal carcinoma: diagnosis and treatment. J Radiol Case Rep 2012;6:9–16.
[57] Eekers DBP, 't Ven L, Deprez S, Jacobi L, Roelofs E, Hoeben A, Lambin P, de Ruysscher D, Troost EGC. The posterior cerebellum, a new organ at risk? Clin TranslRadiat Oncol 2018;8:22–6.
[58] Cantelmi D, Schweizer TA, Cusimano MD. Role of the cerebellum in the neurocognitive sequelae of treatment of tumours of the posterior fossa: an update. Lancet Oncol 2008;9:569–76.
[59] Whaley JT, Kirk M, Cengel K, McDonough J, Bekelman J, Christodouleas JP. Protective effect of transparent film dressing on proton therapy induced skin reactions. Radiat Oncol 2013;24:19.

Please cite this article in press as: Eekers DB et al. The EPTN consensus-based atlas for CT- and MR-based contouring in neuro-oncology. Radiother Oncol (2018), https://doi.org/10.1016/j.radonc.2017.12.013